Soft Matter

COMMUNICATION

Published on 01 April 2016
Licence and permissions

Harnessing viscoelasticity and instabilities for tuning wavy patterns in soft layered composites

Viacheslav Slesarenko and Stephan Rudykh*

Cite this: *Soft Matter*, 2016, 12, 3677

Received 6th December 2015,
Accepted 1st April 2016

DOI: 10.1039/c5sm02949j

www.rsc.org/softmatter

In this study, we combine the elastic instability and non-linear rate-dependent phenomena to achieve microstructure tunability in soft layered materials. In these soft composites, elastic instabilities give rise to formation of wrinkles or wavy patterns. In elastic materials, the critical wavelength as well as amplitude at a particular strain level are exclusively defined by the composite microstructure and contrast in the elastic moduli of the phases. Here, we propose to use rate-dependent soft constituents to increase the admissible range of tunable microstructures. Through the experiments on 3D printed soft laminates, and through the numerical simulation of the visco-hyperelastic composites, we demonstrate the existence of various instability-induced wavy patterns corresponding to the identical deformed state of the identical soft composites.

Natural materials are often found to have complex microstructures that give rise to a large variety of functionalities and desirable properties.[1–4] These design rules have been employed to create bioinspired microstructured materials combining excellent strength and toughness,[5–8] flexibility and protection,[9] or even extremely high adhesion.[10] Moreover, the microstructure defines optical,[11] acoustical,[12] electromechanical,[13] magnetic,[14] and chemical[15] properties of materials. Furthermore, soft composites open the possibility to modify these properties by applied deformations or other external stimuli such as light,[16] heat[17] or magnetic field.[18] This effect can be amplified by the instability-induced microstructure transformations,[19] the phenomenon which is frequently used in nature designed materials. The ability to trigger dramatic microstructure transformations opens exciting opportunities to design soft reconfigurable materials and structures with tunable microstructures[20] to achieve control over a large variety of material properties.[21–24] Recent advances in multi-material three-dimensional printing[25] and other fabrication techniques already allow manufacturing of microstructured materials with resolution comparable to visible light wavelength and even sub-wavelength size.[11] For instance, soft layered composites, when compressed to a critical level, are known to experience elastic instabilities leading to formations of wavy interfaces.[26,27,33] In elastic materials, the critical wavelength as well as amplitude at a particular strain level are exclusively defined by the composite microstructure and contrast in the elastic moduli of the phases. This imposes restrictions on admissible microstructure, and, as a result, the tunability of the material properties and functionalities is limited. To overcome this issue and to increase the admissible range of tunable microstructures, we propose to use rate-dependent soft constituents. This will allow us to design the instabilities by controlling the governing properties of the constituents through the deformation rate. The combination of elastic instabilities and visco-hyperelastic phenomena gives us the access to a rich pool of various instability-induced wavy patterns corresponding to the identical deformed state of the identical soft composites.

Experiments

Layered composite samples with stiff layers and compliant matrix were fabricated using 3D-printer Objet Connex. The available set of digital materials was tested mechanically at various strain rates (from 10^{-4} to 10^{-1} s^{-1}). Through the survey of the material properties, we identified advantageous combinations of constituents to capitalize on the interplay between elastic instabilities and rate-dependent behavior of layered composites. In particular, the soft matrix material was printed in TangoPlus resin (further referred as soft or matrix material), whereas the stiff layers were printed in a digital material (further referred as rigid or layer material), which is a mixture of soft TangoPlus (~65 wt%) and rigid VeroWhite (~35 wt%) resins. For strain rates considered in experiments and numerical simulations (from 10^{-4} to 1 s^{-1}), the elastic modulus of rigid material varies in 8–10 times; while the elastic modulus of soft material is nearly rate-independent. This allows us to increase the range of contrasts in elastic moduli of stiffer and softer constituents and, hence, to achieve an enhanced tunability of the composite microstructures. The material

Department of Aerospace Engineering, Technion – Israel Institute of Technology, Haifa, Israel. E-mail: rudykh@technion.ac.il

Table 1 Material constants

μ_l (MPa)	μ_m (MPa)	α_1	τ_1 (s)	α_2	τ_2 (s)	α_3	τ_2 (s)
22	0.2	0.65	0.15	0.17	4.8	0.1	120

constants of used materials obtained from mechanical testing at different strain rates are summarized in Table 1.

Guided by theoretical and numerical predictions of buckling behavior in rate-independent composites, we examine the composite with stiff phase volume fraction of 15%. The thickness of the stiffer layers is $T_f = 0.75$ mm and the distance between them is $T_m = 4.25$ mm, while the width, height and out-of-plane depth are 85 mm, 35 mm and 8 mm, respectively. The specimens were constrained by special fixtures to eliminate out-of-plane deformation and maintain the plane strain conditions. The composites were subsequently subjected to compression down to 75% of the initial height ($\varepsilon = 25\%$) at the strain rates of 10^{-4}, 10^{-3}, 10^{-2} and 10^{-1} s^{-1}. The compression tests were carried out using Shimadzu EZ-LX testing machine and the strain was measured with a help of a CCD-camera point tracking system.

Modeling

Theoretical studies of buckling in linear elastic layered composites established the foundation for predictions of the onset of buckling and the associated critical wavelengths.[26,28] Nestorović and Triantafyllidis[29] analyzed failure of finitely strained layered composites for quasi-static loadings, and showed the existence of macroscopic and microscopic instabilities. Recently, it was numerically shown, that the triggered wavy microstructures can be used for manipulating elastic waves and inducing band-gaps in dilute laminates,[24] and to increase the large energy dissipation capacity in viscoelastic non-dilute laminates.[30]

Here, we targetly exploit the evolution of microstructure in layered composite with rate-dependent constituents in post-buckling regime to achieve significant tunability of the microstructure. Since the soft material used in 3D-printing can be considered as rate-independent for the strain rates of 10^{-1}–10^{-4} s^{-1}, we approximated its behavior by the neo-Hookean material model. The corresponding strain energy function is

$$W_m(\boldsymbol{C}) = \frac{\mu_m}{2}(I_1(\boldsymbol{C}) - 3), \tag{1}$$

where $I_1(C)$ is the first invariant of the right Cauchy-Green tensor $\boldsymbol{C} = \boldsymbol{F}^T\boldsymbol{F}$, $\boldsymbol{F}$ is the deformation gradient, and μ_m is the shear modulus of matrix. In this case, the second Piola–Kirchhoff stress tensor $\boldsymbol{S}_m$ can be found as

$$\boldsymbol{S}_m = 2\frac{dW_m}{d\boldsymbol{C}} = \mu_m \boldsymbol{I}, \tag{2}$$

where $\boldsymbol{I}$ is the identity tensor. The first Piola–Kirchhoff stress tensor, $\boldsymbol{P}$ can be found as $\boldsymbol{P} = \boldsymbol{FS}$.

To capture the pronounced viscoelastic behavior of the stiffer viscoelastic layers, we implemented Quasi-Linear Viscoelastic (QLV) model.[31,32] Thus, the second Piola–Kirchhoff stress tensor $\boldsymbol{S}_l$ is expressed as

$$\begin{aligned}\boldsymbol{S}_l &= \int_0^t \left[1 - \sum_{i=1}^{n} \alpha_i \left(1 - e^{\frac{s-t}{\tau_i}}\right)\right] \frac{\partial \boldsymbol{S}_l^{el}}{\partial s} ds = \boldsymbol{S}_l^{el}\left(1 - \sum_{i=1}^{n} \alpha_i\right) \\ &+ \sum_{i=1}^{n} \alpha_i \int_0^t e^{\frac{s-t}{\tau_i}} \frac{\partial \boldsymbol{S}_l^{el}}{\partial s} ds,\end{aligned} \tag{3}$$

where $\boldsymbol{S}_l^{el} = \mu_l \boldsymbol{I}$, and μ_l is the shear modulus of the rigid layer material. Prony series parameters, α_i and τ_i, define the rate-dependent behavior of the layers. The properties of the rigid layers were determined from plane strain compressive tests and they are summarized in Table 1. Note that only three terms of Prony series were found to be sufficient to describe the mechanical response of layer material for the considered strain rate range.

To explore the microstructure evolution in the post-buckling regime, the finite element (FE) analysis was employed by means of COMSOL FE code. The QLV material model (eqn (3)) was directly implemented into the numerical solver in terms of the second Piola–Kirchhoff stress tensor. Since several buckling modes are possible during compression, and critical strains for these modes have close values, as we show further, the only buckling mode observed in experiments was taken into account by introduction small imperfection to layers geometry. The 2D representative volume elements (RVE) were constructed, such that they could accommodate the corresponding full buckled wavelength. The response of the composite is computed by applying the periodic displacement boundary conditions.

Results

Experimental observations together with numerical simulations show that for any applied strain rate, buckling occurs when the applied strain reaches the corresponding critical level. Then, the amplitude of the instability-induced wavy patterns increases during a subsequent increase in the compressive strain. Fig. 1a and c show the experimentally observed wrinkling patterns for two strain levels of 15 and 20%, respectively. We observe that the identical composites buckle at different strain levels, defined by applied strain, which leads to the formation of wavy interfaces with different amplitudes for the same strain level. For instance, while buckling already occurs for a relatively fast loading (10^{-1} s^{-1}), the layers stay straight for a slower loading (10^{-4} s^{-1}). Fig. 1b and d show that the numerical simulations also successfully capture this behavior.

Remarkably, we do not observe any effect of strain rate on the buckling wavelength. It is known,[27] that in linear elastic case for the single stiff layer, embedded in soft matrix, the buckling wavelength is related to the contrast in shear moduli as $l \sim (\mu_f/\mu_m)^{\frac{1}{3}}$, where μ_m and μ_f are shear moduli of soft and rigid phases, respectively. However, this relation becomes inaccurate with an increase in volume fraction of the stiff phase.[28] In particular, for composites with incompressible constituents,

 This journal is © The Royal Society of Chemistry 2016

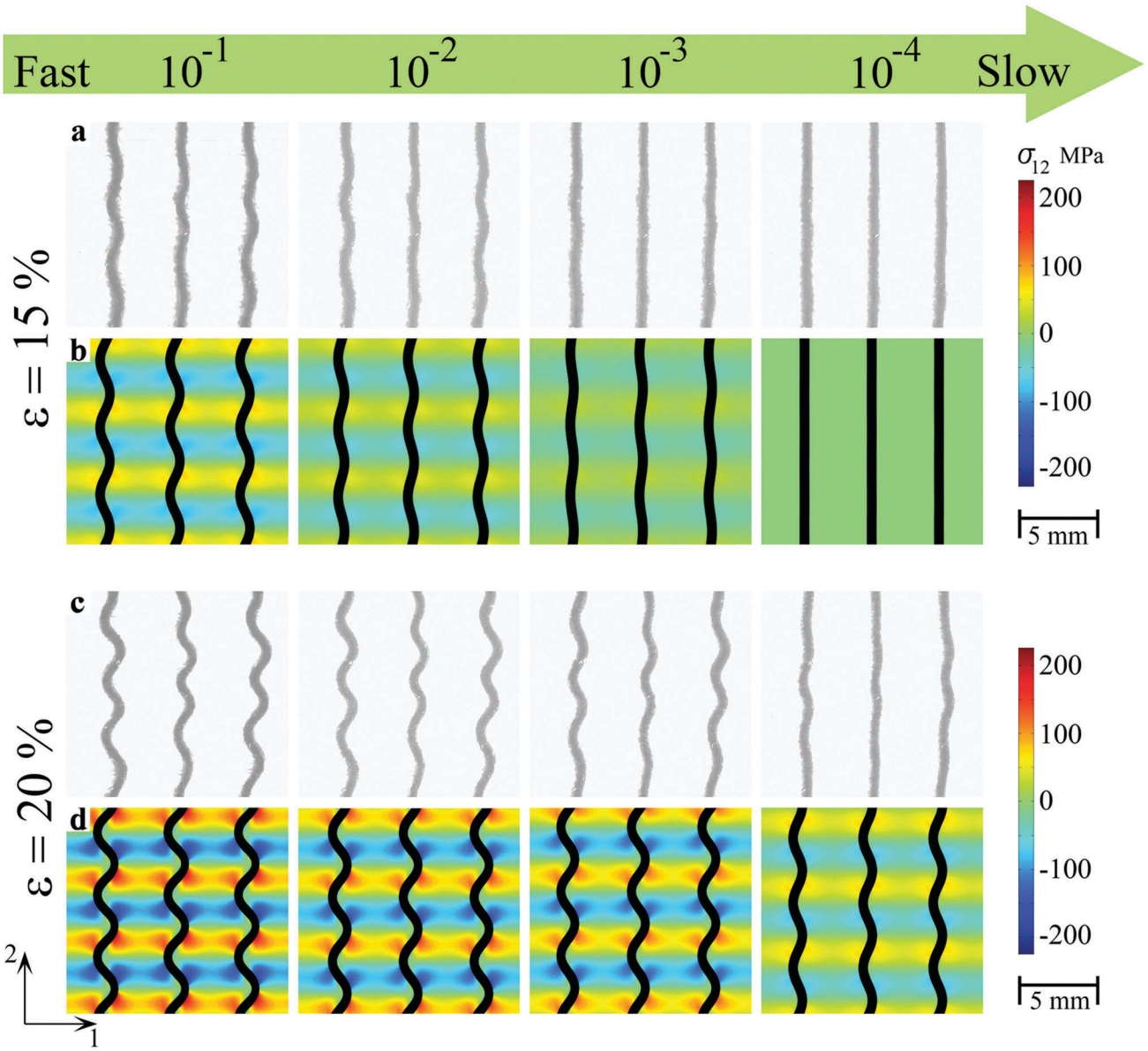


Fig. 1 Formation of wavy interfaces in soft layered composites. (a and c) – Experimentally observed wavy patterns for different strain rates at the strain levels of 15 (a) and 20% (c), respectively. (b and d) – Simulation results, showing σ_{12} stress distribution in matrix for different strain rates at the strain levels of 15 (b) and 20% (d), respectively.

the critical strain for specific buckling mode with wavelength l in plane strain conditions is defined as

$$\varepsilon_b(l) = \frac{1}{2}\frac{\mu_m}{\mu_l}\left(2 + \frac{1}{q_f}\frac{(\sinh(q_m) - q_f\cosh(q_m))^2}{(\sinh(q_m)\cosh(q_m) + q_m)}\right) + \frac{q_f^2}{3}, \quad (4)$$

where q_m and q_f are the normalized thicknesses of matrix and layer respectively, defined as $q_f = \pi T_l/l$, $q_m = \pi T_l/l$. Thus, the critical wavelength of buckling mode is the one corresponding to the minimum value of $\varepsilon_b(l)$.

For viscoelastic materials, which mechanical response depends on the applied strain rate, the effective rate-dependent shear modulus at each point of stress–strain curve can be defined. If the material stress–strain relation is described by the linearized version of the eqn (3), the effective elastic modulus, which depends on the level of applied deformation and strain rate, can be estimated as

$$\mu_{eff}(\varepsilon, \dot{\varepsilon}) = \mu_{eff}^{st} + \mu_{eff}^{visco}(\varepsilon, \dot{\varepsilon}) = \mu_l\left(1 - \sum_{i=1}^{n}\alpha_i\right) + \mu_l\sum_{i=1}^{n}\alpha_i e^{-\frac{\varepsilon}{\dot{\varepsilon}\tau_i}}, \quad (5)$$

where the first term μ_{eff}^{st} is the rate-independent term, while the second term μ_{eff}^{visco} depends on the strain rate. Effective shear modulus μ_{eff} represents the slope of the stress–strain curve for particular strain, and for the loading with constant strain rate the value μ_{eff} attaining the static shear modulus μ_{eff}^{st} at higher levels of strain, when the second term of eqn (5) becomes

infinitely small. For example, for strain rates of 10^{-4} and 10^{-3} s^{-1} the values of the effective shear modulus at the buckling points for rigid material are 1.8 and 2.6 MPa, respectively; while for the strain rate of 10^{-1} s^{-1}, the value of the effective shear modulus is 6.9 MPa. Thus, the contrast between stiff and soft constituent moduli varies from 8.9 to 35 for the considered strain rates. Next, we use the concept of estimated effective moduli for qualitative consideration of the wavelength weak sensitivity observed in our experimental study.

Fig. 2a shows the dependence of the critical strain value on the wavelength for different strain rates. The reported in Fig. 2a critical curves are obtained from eqn (4) with the estimated effective moduli calculated from (5) for experimentally observed buckling strain. We observe that the experimentally determined wavelength corresponds to the minimum in the curve for strain rate 10^{-4} s^{-1}. Note that the critical strain differs only by less than 1.5% from the strain levels corresponding to larger wavelengths. An increase of the strain rate to 10^{-3} s^{-1} leads to a decrease in the critical strain due to higher effective shear modulus. In this case, the minimum strain rate corresponds to slightly higher wavelength, however the calculated and experimentally observed critical strains are very close (compare 16% and 16.05%). Similarly, for a higher strain rate (10^{-2} s^{-1}) we observe that the difference between minimum critical strain and observed critical strain does not exceed 1%. Only for the fastest loading (10^{-1} s^{-1}), the difference between experimentally observed and analytically predicted wavelengths becomes visible. However, it is plausible that the viscoelastic behavior of the matrix material, which has not been accounted for in simulations, starts to play a more significant role for faster loadings. Thus, an increase in the effective shear modulus of matrix material would lead to a decrease in the contrast between phases' moduli, and, may result in a change of the critical curve. Additional potential source, that may affect the experimentally observed buckling behavior, is the presence of interphases and imperfections at the interfaces. These may trigger different buckling modes, especially when the critical strains for these modes are close, as in the considered case. In order to experimentally realize the wavelength tuning, one should consider dilute composites and/or utilize constituents with a significant contrast in instantaneous and infinite elastic moduli. Such composites provide wider range of contrasts between shear moduli of layers and matrix. Moreover, as one can see from Fig. 2b the minima in the corresponding critical curves are

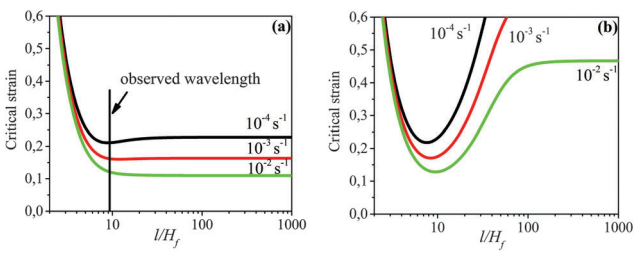


Fig. 2 Critical curves for composites with volume fractions of the stiff phase of 15% (a) and 3% (b).

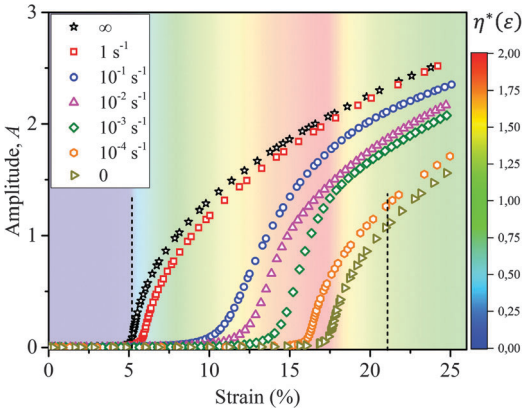


Fig. 3 Dependence of amplitude $A(\varepsilon)$ on strain level for different strain rates. The amplitude is normalized by the stiffer layer thickness. The background color corresponds to the value of the tunability function, $\eta^*(\varepsilon)$. Vertical dashed lines represent the critical strains for instantaneous and infinitely slow loading in the linear elastic case.

more pronounced, which allows to trigger different buckling modes for different rates of loading. In the following, we focus on the microstructure tunability of the composites with weak wavelength tuning. In this case, the microstructure tunability is due to the tailored onset of buckling, resulting in targeted post-buckling amplitudes of wavy interfaces.

Fig. 3 shows the dependence of the amplitude, $A(\varepsilon)$, normalized by the initial thickness of the stiff layer, on the applied strain in the assumption of the same buckling mode. We observe a rapid increase in the wrinkling amplitude directly after the buckling; however, after the formation of the wavy patterns, the corresponding curves flatten with further increase in compressive loading. Obviously, at each macroscopic strain level, different amplitudes can be induced by managing the strain rate. At the same time, considering the strain rates which is slower than 1 s^{-1} (red squares on Fig. 3) and faster than 0.1 s^{-1} (blue circles), one may notice that variety of achievable amplitudes for strain of 10% is much wider ($0.1 < A(\varepsilon) < 1.1$) in comparison with strain of 20% ($1.9 < A(\varepsilon) < 2.1$). To quantify this tunability phenomena, we introduce function, $\eta(\varepsilon,\dot{\varepsilon}_{\min},\dot{\varepsilon}_{\max})$, which describes the tuning capability for specific strain value ε and for strain rates range $[\dot{\varepsilon}_{\min},\dot{\varepsilon}_{\max}]$

$$\eta(\varepsilon,\dot{\varepsilon}_{\min},\dot{\varepsilon}_{\max}) = A(\varepsilon)|_{\dot{\varepsilon}=\dot{\varepsilon}_{\max}} - A(\varepsilon)|_{\dot{\varepsilon}=\dot{\varepsilon}_{\min}} \quad (6)$$

The defined tuning capability function can be expanded to capture any possible strain rates. In this case, eqn (6) is modified as

$$\eta^*(\varepsilon) \equiv \eta(\varepsilon,0,\infty) = A(\varepsilon)|_{\dot{\varepsilon}\to\infty} - A(\varepsilon)|_{\dot{\varepsilon}\to 0} \quad (7)$$

Fig. 4a and b show the dependence of the function $\eta(\varepsilon,\dot{\varepsilon}_{\min},\dot{\varepsilon}_{\max})$ on the strain for the various ranges of strain rates $[\dot{\varepsilon}_{\min}, \dot{\varepsilon}_{\max}]$. We observe that the tuning capability is non-monotonic function, and it reaches the maximum for a particular strain level $\varepsilon_p(\dot{\varepsilon}_{\min},\dot{\varepsilon}_{\max})$. The behavior of viscoelastic materials can be considered as rate-independent under infinitely fast (instantaneous) or infinitely slow loadings. In these extreme cases, the effective shear modulus of the layer reduces to μ_1 and $\mu_{\text{eff}}^{\text{st}}$, respectively.

This journal is © The Royal Society of Chemistry 2016

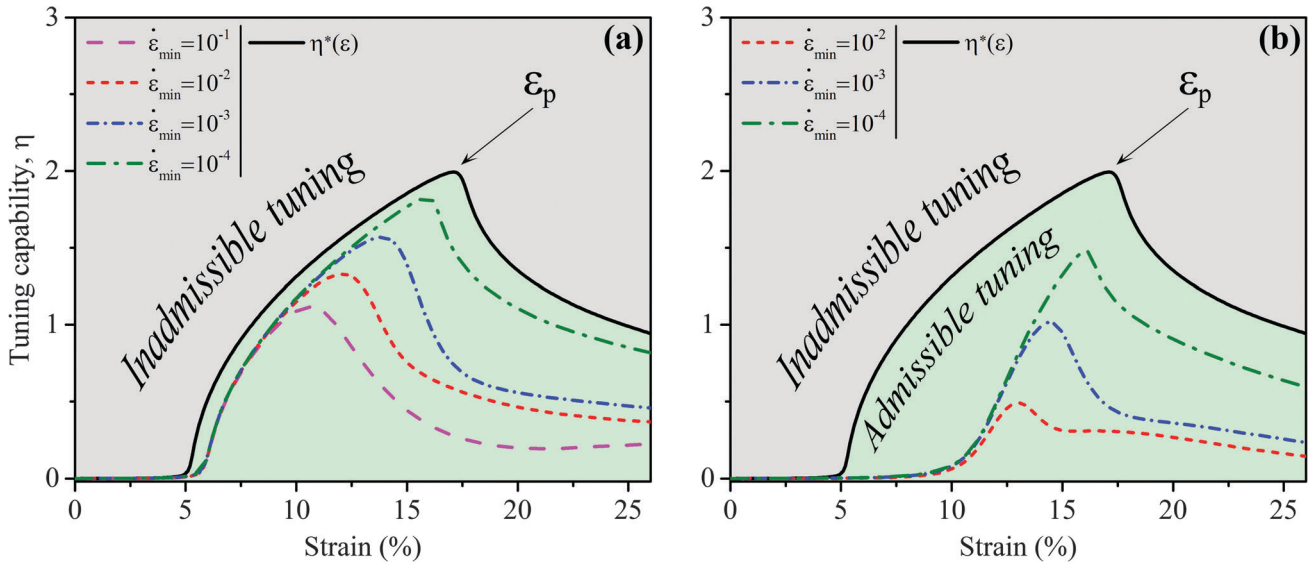


Fig. 4 Dependence of tuning capability $\eta(\varepsilon,\dot{\varepsilon}_{min},\dot{\varepsilon}_{max})$ on strain for different sets of $\dot{\varepsilon}_{min}$ for $\dot{\varepsilon}_{max}$ = 1 s^{-1} (a) or $\dot{\varepsilon}_{max}$ = 0.1 s^{-1} (b).

Thus, by using eqn (4), one can predict the critical strain in these cases. The corresponding estimates are shown in Fig. 3 by the dashed vertical lines. We observe that the approximation is in a good agreement with simulation data for instantaneous loading. However, the difference between the theoretical estimation and simulation results for infinitely slow loading is more significant. This is due to the fact, that in this regime, the buckling appears at large strains where nonlinear effects, which are not accounted in the analytical estimate, become significant. These cases of infinitely slow and infinitely fast loading provide the estimates for the bounds for the microstructure tunability. Thus, for each strain rates $\dot{\varepsilon}_{min}$ and $\dot{\varepsilon}_{max}$, we have $\eta(\varepsilon,\dot{\varepsilon}_{min},\dot{\varepsilon}_{max}) < \eta^*(\varepsilon)$. Therefore, the area under the corresponding curve in Fig. 4a and b (black) encloses the admissible values of the tuning capability in layered composites. While the tuning capability is limited by the value of η^* function, the exact value of ε_p is defined by the material constants, in particular, by the Prony series constants such as relaxation times τ_i. Consequently, by combining different materials pairs for composite constitutions one may achieve maximal tunability for the specific strain ranges.

Conclusions

We investigated the elastic instability phenomenon as well as the post-buckling behavior of soft layered composites subjected to compression. Through the experiments on finitely deformed 3D-printed composites and through the numerical simulations, it was shown that for composites with visco-hyperelastic constitutes the critical strain significantly depends on the strain rate. Moreover, we revealed the mechanism that governs the formation and tunability of wavy patterns. We find that the combination of the elastic instability and visco-hyperelastic phenomena leads to a significant increase the admissible range of tunable microstructures. We found that the tuning capability reaches its maximum for particular strain level, which, in turn, depends on the composite microstructure as well as on the material properties of the constituents. Consequently, the composites with viscoelastic constituents can be directly tailored to achieve required microstructure tunability. This can provide powerful means to control the material performance and achieve new functionalities.

Acknowledgements

This research was supported by the ISRAEL SCIENCE FOUNDATION (grants 1550/15 and 1973/15) and Ministry of Defense under contract 4440687560. SR gratefully acknowledges the support of Taub Foundation through the Horev Fellowship – Leaders in Science and Technology.

References

1 C. Levi, J. L. Barton, C. Guillemet, E. Bras and P. Lehuede, *J. Mater. Sci. Lett.*, 1989, **8**, 337–339.
2 S. Kinoshita and S. Yoshioka, *ChemPhysChem*, 2005, **6**, 1442–1459.
3 C. Sanchez, H. Arribart and M. M. G. Guille, *Nat. Mater.*, 2005, **4**, 277–288.
4 K. Koch, B. Bhushan and W. Barthlott, *Soft Matter*, 2008, **4**, 1943.
5 L. S. Dimas, G. H. Bratzel, I. Eylon and M. J. Buehler, *Adv. Funct. Mater.*, 2013, **23**, 4629–4638.
6 A. R. Studart, *Adv. Mater.*, 2012, **24**, 5024–5044.
7 A. Finnemore, P. Cunha, T. Shean, S. Vignolini, S. Guldin, M. Oyen and U. Steiner, *Nat. Commun.*, 2012, **3**, 966.
8 C. Ortiz and M. C. Boyce, *Science*, 2008, **319**, 1053.
9 S. Rudykh, C. Ortiz and M. C. Boyce, *Soft Matter*, 2015, **11**, 2547–2554.
10 M. K. Kwak, C. Pang, H.-E. Jeong, H.-N. Kim, H. Yoon, H.-S. Jung and K.-Y. Suh, *Adv. Funct. Mater.*, 2011, **21**, 3606–3616.

11 M. Kolle, A. Lethbridge, M. Kreysing, J. J. Baumberg, J. Aizenberg and P. Vukusic, *Adv. Mater.*, 2013, **25**, 2239–2245.
12 S. Zhang, C. Xia and N. Fang, *Phys. Rev. Lett.*, 2011, **106**, 024301.
13 S. Rudykh, A. Lewinstein, G. Uner and G. deBotton, *Appl. Phys. Lett.*, 2013, **102**, 151905.
14 E. Galipeau, S. Rudykh, G. deBotton and P. Ponte Castañeda, *Int. J. Solids Struct.*, 2014, **51**, 3012–3024.
15 F. Hibbe, C. Chmelik, L. Heinke, S. Pramanik, J. Li, D. M. Ruthven, D. Tzoulaki and J. Kärger, *J. Am. Chem. Soc.*, 2011, **133**, 2804–2807.
16 T. M. Conjugated and R. Langer, *Nature*, 2005, **434**, 695–697.
17 M. Behl and A. Lendlein, *Soft Matter*, 2007, **3**, 58.
18 R. Geryak and V. V. Tsukruk, *Soft Matter*, 2014, **10**, 1246–1263.
19 A. J. Crosby, *Soft Matter*, 2010, **6**, 5660.
20 T. Su, J. Liu, D. Terwagne, P. M. Reis and K. Bertoldi, *Soft Matter*, 2014, **10**, 6294–6302.
21 S. Singamaneni and V. V. Tsukruk, *Soft Matter*, 2010, **6**, 5681.
22 G. P. McKnight and C. P. Henry, *Proc. SPIE*, 2008, **6929**, 692919.
23 C. P. Henry and G. P. McKnight, *Proc. SPIE*, 2006, **6170**, 617023.
24 S. Rudykh and M. C. Boyce, *Phys. Rev. Lett.*, 2014, **112**, 034301.
25 X. Zheng, H. Lee, T. H. Weisgraber, M. Shusteff, J. DeOtte, E. B. Duoss, J. D. Kuntz, M. M. Biener, Q. Ge, J. A Jackson, S. O. Kucheyev, N. X. Fang and C. M. Spadaccini, *Science*, 2014, **344**, 1373–1377.
26 B. W. Rosen, *Fiber Compos. Mater. Soc. Met. Semin.*, 1967, 37–75.
27 Y. Li, N. Kaynia, S. Rudykh and M. C. Boyce, *Adv. Eng. Mater.*, 2013, **15**, 921–926.
28 R. Parnes and A. Chiskis, *J. Mech. Phys. Solids*, 2002, **50**, 855–879.
29 M. D. Nestorović and N. Triantafyllidis, *J. Mech. Phys. Solids*, 2004, **52**, 941–974.
30 K. Alur and J. Meaud, *Int. J. Solids Struct.*, 2015, **72**, 130–143.
31 R. De Pascalis, I. D. Abrahams and W. J. Parnell, *Proc. R. Soc. A*, 2014, **470**, 20140058.
32 Y. C. Fung, *Biomechanics: mechanical properties of living tissues*, Springer-Verlag, New York, 1981.
33 E. Lejeune, A. Javili and C. Linder, *Soft Matter*, 2016, **12**, 806–816.

 This journal is © The Royal Society of Chemistry 2016